INTERNATIONAL JOURNAL FOR NUMERICAL METHODS IN FLUIDS
Int. J. Numer. Meth. Fluids **30**: 257–277 (1999)

COMPUTATIONAL STUDY OF CURVED SHOCK–VORTEX INTERACTION

A. CHATTERJEE* AND A. POVITSKY[1]

Faculty of Aerospace Engineering, Technion-Israel Institute of Technology, Haifa 32000, Israel

SUMMARY

The interaction between a curved shock wave and a compressible vortex is numerically investigated. The investigation concentrates on the local deformation of the shock structure due to the shock–vortex interaction. The essentially non-oscillatory (ENO) scheme is used to solve the unsteady two-dimensional Euler equations. A curved shock wave is obtained by the diffraction of an initially planar shock wave around a right-angled corner and then allowed to interact with a strong compressible vortex superimposed on the flow. The same vortex affects the shock wave differently depending on the placement of the vortex because of the varying strength of the shock wave. This effect could range from a non-symmetric deformation of the shock wave to a local disruption in the shock structure depending on the strength of the shock wave in the interaction region. This process leading to a local disruption in the shock structure is analyzed in detail. It is shown that such a disruption in the shock structure can be predicted by simple one-dimensional considerations. Copyright © 1999 John Wiley & Sons, Ltd.

KEY WORDS: Euler equations; ENO scheme; shock–vortex interaction; shock deformation; shock disruption

1. INTRODUCTION

Shock wave–vortex interactions have been a fertile field of investigation for several decades. The previous experimental approach to these investigations has given way to a more numerical approach in this decade. These numerical investigations have been greatly facilitated by the evolution of high resolution shock-capturing schemes. Shock wave–vortex interactions are of fundamental importance in diverse fields, such as noise production in high-speed aircraft, in turbulence amplification by shock waves and in the interaction between mixing zones and shock waves among other applications.

Shock–vortex interactions can be broadly classified into weak and strong interactions. Weak interactions involve slight deformation of the shock wave and the acoustic wave generated can be predicted by linear theories and simulated using simple numerical techniques. Strong interactions involve significant deformation of the shock wave by the vortex and may include the production of secondary shocks. Linear theories are no longer applicable and high resolution shock-capturing schemes are required for accurate numerical simulation of this strongly non-linear phenomenon.

* Correspondence to: CFD Group, Aeronautical Development Agency, PB 1718, Vimnapura Post, Bangalore 560017, India. Fax: +91 80 5234493; e-mail: avijit@ada.ernet.in
[1] Current address: ICASE, NASA Langley Research Center, Hampton, VA, USA.

CCC 0271–2091/99/110257–21$17.50

Received June 1997
Revised April 1998

Both the strong and weak shock–vortex interactions have been studied numerically in the frame work of the Euler equations [1,2] and by a direct numerical simulation [3]. These studies generally involved the numerical simulation of the interaction between a vortex and a planar shock wave.

In real life applications, the shock wave interacting with a vortex can often be non-planar. This work is concerned with the numerical investigation of the interaction between a compressible vortex and a curved shock wave. The numerical simulations are two-dimensional and solve the Euler equations defining inviscid compressible flow. The significantly larger time scales for viscous dissipation as compared with other important time scales involved in shock–vortex interactions makes it possible to neglect viscous effects in numerical computations [2]. A high resolution shock-capturing scheme in the form of the essentially non-oscillatory (ENO) scheme [4,5] is used to solve for the unsteady Euler equations. The dual capacity of ENO schemes for high-order accuracy along with non-oscillatory shock capturing makes the ENO schemes especially attractive for modeling a complex interaction involving a shock wave—that of a curved shock wave interacting with a strong compressible vortex.

The curved shock wave is obtained by diffracting an incident planar shock wave around a right-angled corner and this is allowed to interact with a compressible vortex superimposed on the flow. The authors concentrate on investigating the local deformation of the shock structure especially in the interaction region. The curved shock wave undergoes a typical modification to its structure in the presence of a vortex depending upon the clockwise or counter-clockwise orientation of the vortex. Because of the varying strength of the shock wave, the same vortex could produce a very different effect on the shock structure in the interaction region depending on the location of the vortex. A vortex that causes a non-symmetric deformation of the shock wave if the interaction region consisted of the relatively stronger part of the shock could cause a local disruption in the shock structure if the interaction region was at a different and weaker part of the shock wave. This disruption is of a temporary nature and the shock wave subsequently regains its definition.

Such a local disruption in the shock structure has been observed in experimental investigations involving a planar shock wave with a two-dimensional compressible vortex [6], as well as in the more complicated interaction of shock waves with a cavity [7], where curved reflected shock waves interact with the compressible vortex generated by shock wave diffraction. This phenomenon of a local disruption in the shock wave when interacting with a strong compressible vortex has not been studied previously and in this work the process leading to a local disruption in the shock structure, especially for a curved shock wave, is analyzed in detail. It is also shown that such disruptions can be predicted by simple one-dimensional considerations.

2. GOVERNING EQUATIONS AND NUMERICAL TECHNIQUE

The two-dimensional unsteady Euler equations of gas dynamics describing inviscid compressible flow in the differential and conservative form can be written as:

$$\boldsymbol{u}_t + \boldsymbol{f}_x + \boldsymbol{g}_y = 0. \tag{1}$$

The vectors in Equation (1) are

$$\boldsymbol{u} = \begin{pmatrix} \rho \\ \rho u \\ \rho v \\ e \end{pmatrix}, \qquad \boldsymbol{f} = \begin{pmatrix} \rho u \\ \rho u^2 + p \\ \rho uv \\ (e+p)u \end{pmatrix}, \qquad \boldsymbol{g} = \begin{pmatrix} \rho v \\ \rho uv \\ \rho v^2 + p \\ (e+p)v \end{pmatrix}, \tag{2}$$

in which ρ is density, p is static pressure, (u, v) is the velocity in Cartesian co-ordinates (x, y), and e is the total energy, related to the other variables by an equation of state, which for a perfect gas, is

$$e = \frac{p}{(\gamma - 1)} + \frac{1}{2}\rho(u^2 + v^2), \tag{3}$$

where γ is the ratio of specific heats ($= 1.4$).

The Euler equations in the above form are solved by the ENO [4,5] scheme. The ENO scheme is able to maintain a high-order accuracy as well as provide for non-oscillatory shocks by using an adaptive stenciling procedure. The points in the stencil that contribute to the computation of numerical fluxes at cell interfaces for the next time step are chosen in a non-linear manner and depend on the instantaneous solution. This choice attempts to make use of the smoothest possible information in the computation of the fluxes. In this work the ENO scheme used is in the ENO-Roe form [8,9] and has the ENO construction procedure based on the numerical fluxes rather than on cell averages of the state variables. An explicit form is used to solve this time-dependent flow and advancement in time is by a Runge–Kutta type TVD time integration [8,9]. The ENO-Roe form along with a TVD Runge–Kutta time discretization belongs to the class of efficient implementation for ENO schemes and are much easier to implement especially for multi-dimensional cases as compared with the original ENO schemes [4,5] with the ENO construction procedure based on cell averages and a Lax–Wendroff procedure for the time discretization.

The ENO-Roe scheme is based on the first-order Roe scheme and thus will admit entropy violating expansion shocks. To prevent entropy violating solutions the 'entropy fix' described in [9] is used. Computing unsteady shock waves by high resolution shock-capturing schemes result in the generation of spurious entropy [10,11]. But it has been shown [11] that pressure waves remain unaffected by the numerical entropy generation to the extent that even acoustic computations are not likely to be affected by this phenomenon. Thus, the effect of the numerical entropy generation on the type of flow phenomenon being considered in the present study of shock wave–vortex interaction should be negligible.

Unless otherwise specified, a third-order accuracy in space and a second-order accuracy in time was used. All numerical investigations involved a moving shock wave and in the initial configuration the shock was planar. The initial conditions behind the shock are prescribed according to the Rankine–Hugoniot relations, while ambient conditions are given ahead of it. Characteristic boundary conditions based on Riemann invariants are prescribed at open boundaries and reflection boundary conditions at the solid boundaries. Regular fixed Cartesian grids were used and unless stated consisted of 300×300 grid points. The problems of accuracy related to the order of the numerical scheme and the discretization used, including a grid refinement study is discussed in a later section.

3. INTERACTION OF CURVED SHOCK WITH A VORTEX

A detailed numerical investigation in which a curved shock wave interacts with a compressible vortex superimposed on the flow is carried out. The curved shock wave is obtained by diffracting an incident planar shock wave around a right-angled corner. Such a diffraction produces a curved shock wave separating two regions in which the shock wave is plane. The two regions containing a planar shock are the plane undisturbed part of the incident shock at the top and a 'wall shock' at the bottom that is perpendicular to the wall and tangent to the curved shock [12]. This is shown schematically in Figure 1. The strength of the curved part of the shock is maximum at the top where it meets the plane undisturbed incident shock and it decreases thereafter, but at no place does it become vanishingly weak even for low Mach numbers [12].

The shock wave proceeds into ambient conditions and interacts with a compressible vortex superimposed on the ambient state, as shown in Figure 1. The vortex generated is similar to those in [1,2]. The vortex model consists of two regions of vortical flow; an inner core region consisting of uniform velocity and a surrounding region where the velocity gradually goes to zero. This is represented by

$$U_\theta(r) = U_c, \quad r < R_c, \tag{4}$$

$$U_\theta(r) = Ar + \frac{B}{r}, \quad R_c \le r \le R_o, \tag{5}$$

where U_θ is the tangential velocity, U_c the constant core velocity, r the distance from vortex center, R_c the vortex core radius, R_o the outer radius.

The coefficients A and B in Equation (5) are chosen so that U_θ equals U_c when r equals R_c and U_θ equals 0 when r equals R_o. The values for pressure and density in the vortex are taken to be the same as those in the ambient (as in [1]). The tangential velocity, density and pressure distribution in the vortex tends towards that measured experimentally for a freely moving

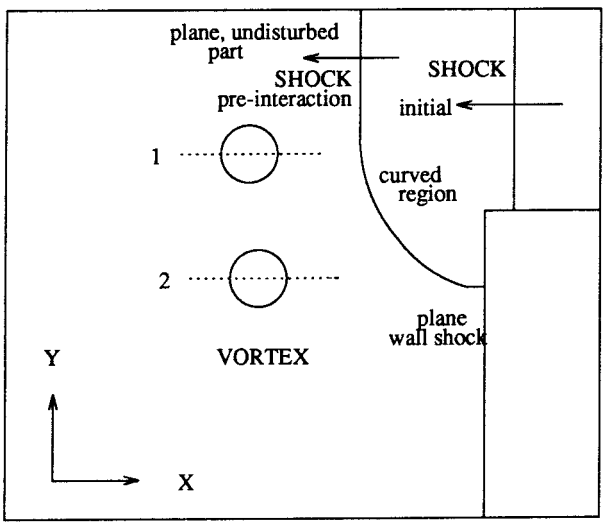

Figure 1. Initial conditions and geometry for curved shock–vortex interactions.

Table I. Conditions for curved shock–vortex interactions

Test case	Vortex center		Approximate Mach number		
	X	Y	$Y+R_c$	Y	$Y-R_c$
1	0.5	1.3	1.5	1.5	1.43
2	0.5	0.7	1.33	1.27	1.2

compressible vortex [6] by the time of the shock–vortex interaction, and this is discussed in a later section.

The physical domain, which is the same as the computational domain along with the initial conditions, is shown in Figure 1. The total dimensions are 1.2 in the x-direction and 2.0 in the y-direction. The right-angled corner extends from $x = 1.0$ to $x = 1.2$ and from $y = 0$ to $y = 1.0$. In all cases the planar shock was at $x = 1.1$ at the start of the simulations and it proceeds from right to left. The vortex has a core radius $R_c = 0.15$ and an outer radius $R_o = 0.3$. Two different sets of simulations with the vortex center at different heights are discussed, the positions of the vortex centers are listed in Table I and also shown in Figure 1.

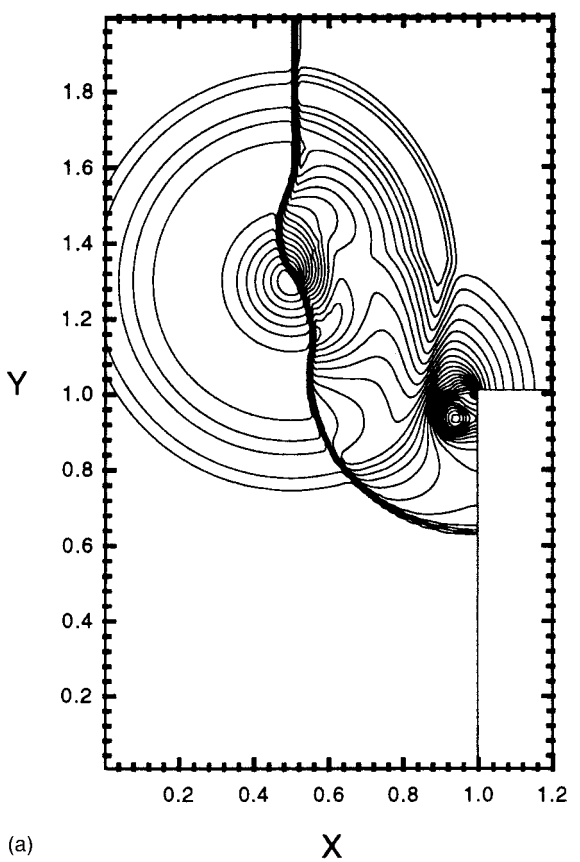

Figure 2. Pressure contours for test case 1 with counter-clockwise rotating vortex at normalized times (T); (a) $T = 0.52$, (b) $T = 0.62$, (c) $T = 0.71$.

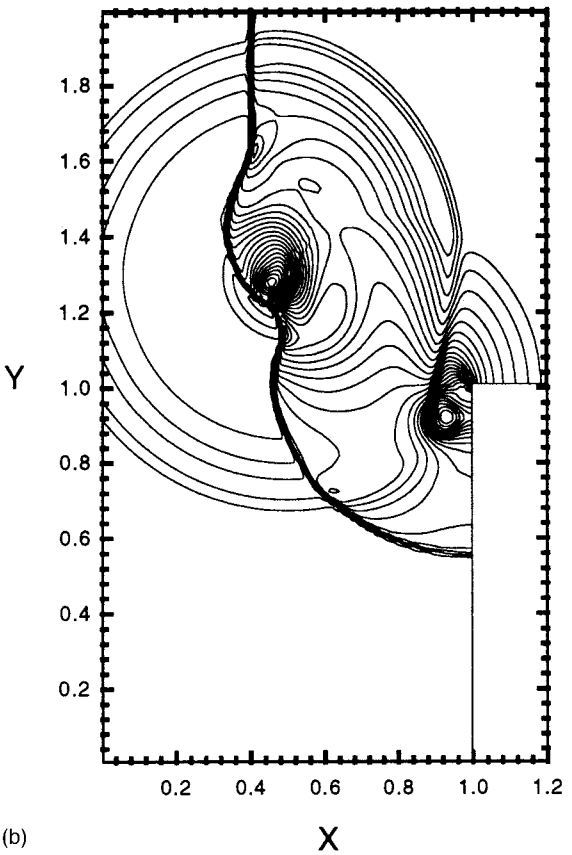

Figure 2 (*Continued*)

In all cases considered, the incident planar shock wave had a Mach number of 1.5, which implied subsonic conditions behind the shock with a Mach number 0.6. The constant core velocity U_c equalled the velocity of the fluid behind the incident planar shock. This value for the core velocity U_c has been the basis for a strong interaction involving a planar shock wave of similar magnitude and a compressible vortex in Reference [2]. The approximate Mach number for the diffracting shock wave (undisturbed by a superimposed vortex) at positions corresponding to the center of the superimposed vortex as well as two points distances R_c above and below the vortex centers for the two test cases discussed are given in Table I.

The initial placement of the planar shock wave and the vortex dimensions ensures that the diffracted shock wave encounters the vortex before the presence of the solid boundaries begin to affect the vortex. It is assumed that the vortex produced due to flow separation at the right-angled corner behind the diffracting shock does not affect the qualitative character of the shock–vortex interaction being investigated. This is a reasonable assumption considering the localized nature of this vortex at the corner during the interaction period and the distance between the shock–vortex interaction region and this vortex.

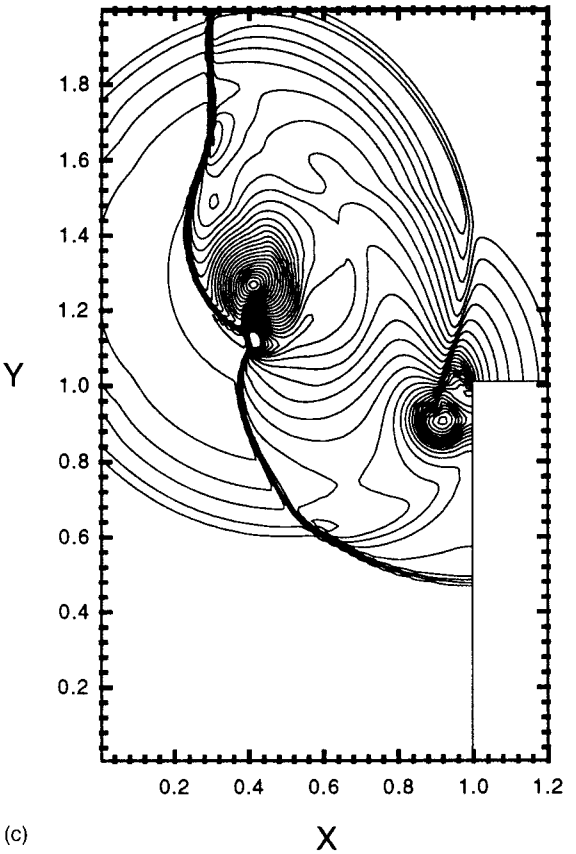

Figure 2 (*Continued*)

4. NUMERICAL RESULTS

The first test case pertains to the vortex center placed at $x = 0.5$ and $y = 1.3$. This implies that in the interaction region, the shock wave is almost planar consisting mostly of the plane undisturbed part of the incident shock. The results are similar to those for a strong interaction between planar shocks and a compressible vortex discussed in [1,2]. The interaction process is also discussed in detail in [3]. Results in this and the subsequent test case are shown in terms of pressure contours and consist of 30 contour lines at equal intervals.

Figure 2(a)–(c) show results for a counter-clockwise rotating vortex at normalized times of 0.52, 0.62 and 0.71 respectively. When the shock wave enters the vortical region, the part of the shock in the interaction region where the shock velocity is opposed by the vortex rotation propagates slower than the part where the shock velocity is supported by the vortex rotation. In this particular case, the bottom half of the shock in the interaction region meets an opposing flow and propagates slower than the top half, which encounters a flow in the same direction as the propagating shock wave. This initially implies a symmetric deformation of the shock, as seen in Figure 2(a). There is also a strengthening of the part of the shock wave in the interaction region where the advancing shock faces an opposing flow due to an increase in the relative Mach number (relative to the oncoming flow) of this part of the shock and a

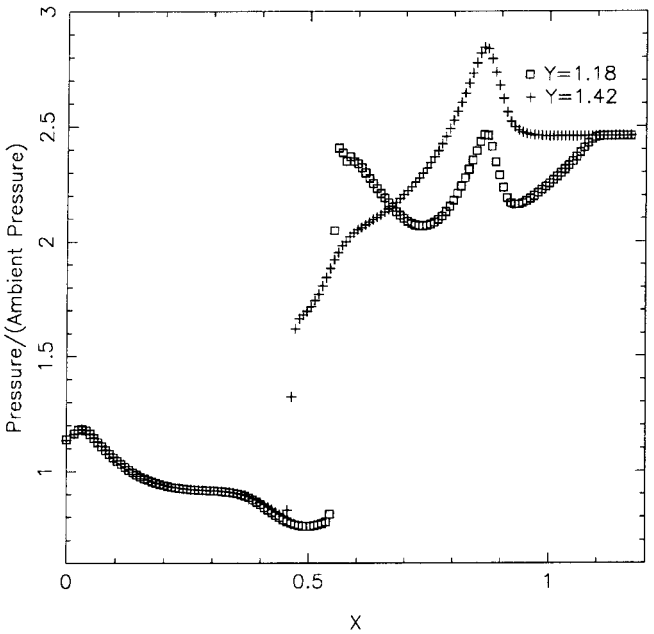

Figure 3. Pressure variation for test case 1 ($T = 0.52$).

similar weakening of the part of the shock in the interaction region where the vortical velocity is in the same direction as that of the shock due to a decrease in its relative Mach number (relative to the oncoming flow). This non-uniform jump across the shock means a distortion of the initial vortex leading to a more non-symmetric distortion of the shock, this can be seen in Figure 2(b). The additional pressure gradients that appear parallel to the shock produce secondary shock structures both of which are attached to the shock, as seen in Figure 2(c). These secondary shock structures are in the form of a Mach structure that agrees with observations in [2] regarding the formation of a Mach structure in the later stages of an interaction of a relatively strong shock with a compressible vortex. The shock will gradually relax to its original form as the vortex is left behind.

Figure 3 shows the pressure variation along the x-direction at $y = 1.18$ and $y = 1.42$ both equidistant from the vortex center ($y = 1.3$) at a normalized time of 0.52. This situation corresponds to a symmetric deformation of the shock, as shown in Figure 2(a). At $y = 1.18$ and $y = 1.42$, the shock is almost normal to the x-axis and is also respectively stronger and weaker due to the change in the relative Mach number because of the interaction with the vortex. Assuming the shock to be spread over one grid point for this third-order ENO scheme, the pressure ratios across the shock are approximately 3.0 at $y = 1.18$ and 1.97 at $y = 1.42$. The plane undisturbed shock had a Mach number of 1.5 corresponding to a pressure ratio of 2.45. From the Rankine–Hugoniot relations the relative Mach number at the stronger part of the shock ($y = 1.18$) is 1.64 and the relative Mach number at the weaker part ($y = 1.42$) is 1.35. Thus, this indicates the shock undergoing an almost symmetrical deformation at that time.

In the second test case considered, the vortex center was at $x = 0.5$ and $y = 0.7$. The shock structure in the interaction region is totally curved and on average at a weaker strength than the earlier test case with the shock strength decreasing along the curved shock from the top onwards. Results are presented for the counter-clockwise and clockwise rotation of the vortex.

First the counter-clockwise case will be discussed. Figure 4(a) at a normalized time 0.52 shows the shock wave profile before the shock has entered the vortical region. Figure 4(b) at normalized time 0.66 shows the modified shock profile due to the vortical velocity field. The velocity field of the vortex when added to that of the curved shock results in the upper part of the shock wave in the interaction region traveling faster than the lower part. This results in a pulling forward of the upper part of the shock and depressing the lower part. Compounded with the fact that the shock was already curved to start with, this implies a tendency on the part of the shock to become almost horizontal to the x-axis in the interaction region, as in Figure 4(b).

Because of the shock as a whole being relatively weaker in the interaction region compared with the previous test case, there is a further decrease in the relative Mach number of the shock in the part of the core region where the vortical velocity is in the same direction as that of the velocity of the shock. Since the shock front is almost parallel to the x-axis in the interaction region, the lowest relative Mach number for the shock front will occur where it is almost aligned with the vortex diameter, which is parallel to the x-axis. At this position, a situation occurs where to the left of the vortex center, the direction of the vortical velocity almost matches that of the shock velocity in the interaction region. The resulting decrease in the relative Mach number of the shock could lead to a local disruption in the shock structure as

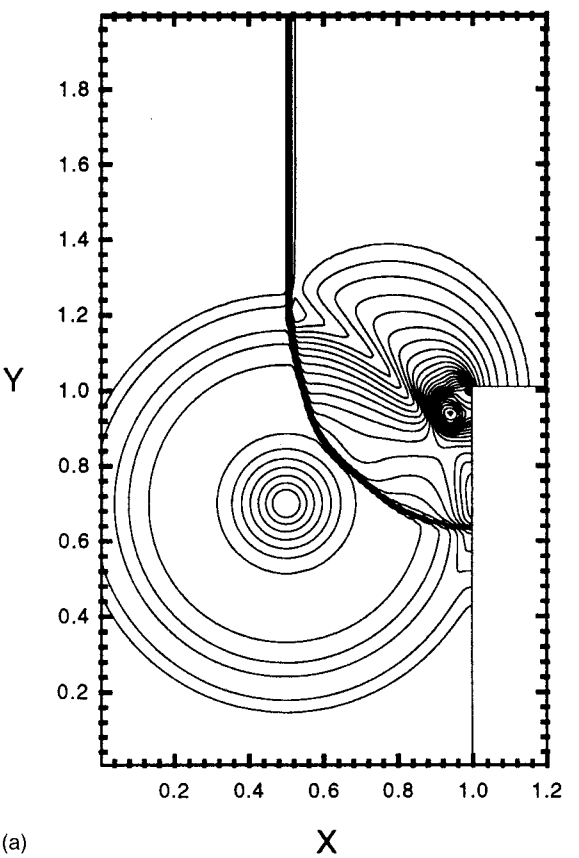

Figure 4. Pressure contours for test case 2 with counter-clockwise rotating vortex; (a) $T = 0.52$, (b) $T = 0.66$, (c) $T = 0.76$, (d) $T = 0.85$, (e) $T = 1.04$.

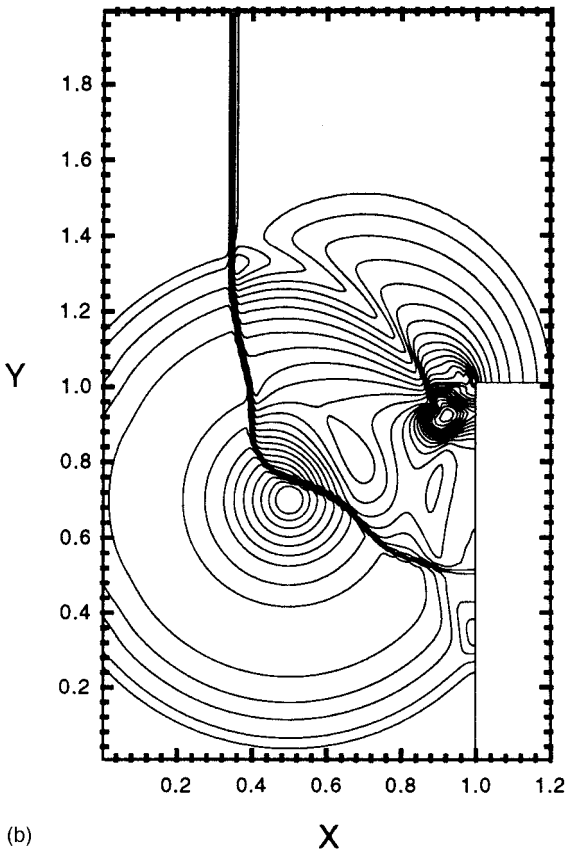

Figure 4 (*Continued*)

encountered here. Figure 4(c) at normalized time 0.76 shows the disruption in the shock wave at and near left of the vortex center. The shock remains disrupted in the third (bottom left) quadrant of the vortex. Figure 4(d) shows the still disrupted shock wave at a normalized time 0.85. Figure 4(e) at a normalized time 1.04 shows the resulting shock structure including secondary shocks after the vortex is crossed. The absence of a Mach stem in the secondary shock structures, and the presence of a triple point where the secondary structures meet is again in agreement with observations in [2,3] concerning the later stages of the interaction between a relatively weaker shock and a compressible vortex.

In the clockwise case (see Figure 5), the initial shock structure (same as in Figure 4(a)) is acted upon by the vortical velocity field and modifications to it make it approach the vortex center almost normal to the x-axis. This is a result of the upper part of the curved shock being held back and the lower part pulled forward. Because of this, the lowest relative Mach number for the shock front occurs when it is almost aligned with the vortex diameter, which is parallel to the y-axis. In this position, a situation again arises below the vortex center where the direction of the vortical velocity almost matches that of the shock front in the interaction region. This causes a sufficient decrease in the relative Mach number to produce a local disruption in the shock structure. Figure 5(a) at a normalized time 0.76 shows the disruption in the shock wave. Again the shock remains disrupted in the third quadrant of the vortex and

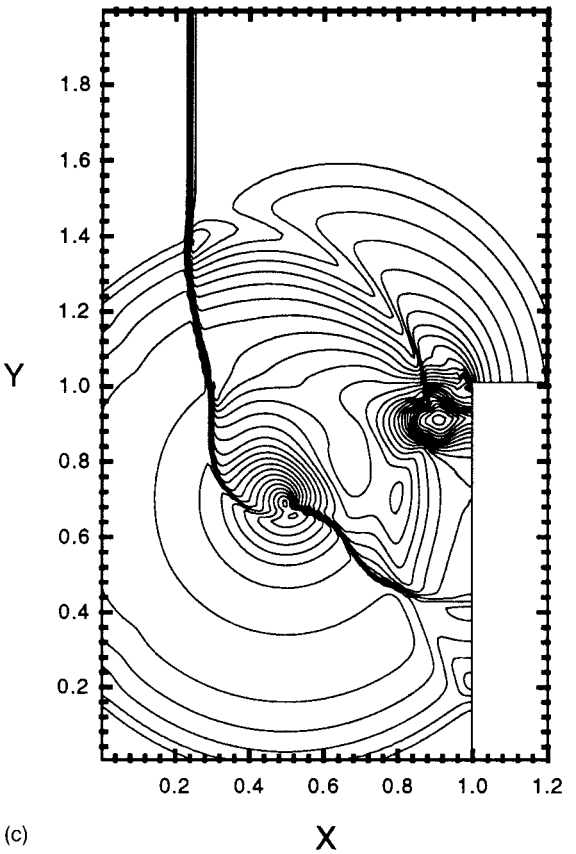

Figure 4 (*Continued*)

reunites after the vortex is crossed. Figure 5(b) at a normalized time 1.04 shows the reunited shock with secondary structures as in the counter-clockwise case.

In a qualitative sense, the basic shock–vortex interaction is the same regardless of a clockwise or a counter-clockwise orientation of the vortex. But the two interactions performed with a clockwise and a counter-clockwise rotating vortex serves to better illustrate the basic premise that a shock wave encountering a component of the vortical velocity field in the direction of the shock wave propagation can weaken the shock wave to an extent that a local disruption in the shock structure takes place.

The disruption in the shock wave (for a counter-clockwise rotating vortex at a normalized time of 0.76), captured on a discretization of 600×600 grid points using an ENO scheme of the same spatial and temporal accuracy, is shown locally for the vortex and vortex core region in Figure 6(a) and (b) respectively. A local disruption in the shock front can again be discerned.

In Figure 7(a) the pressure variation along the y-axis at discrete points is shown for the counter-clockwise rotating vortex of the second test case at a normalized time of 0.76 (corresponding to a local disruption in the shock structure). These variations are at three x-stations corresponding to the center of the vortex at $x = 0.5$ and at equidistant points $x = 0.42$ and $x = 0.58$ from the center. At these points, the shock is almost normal to the

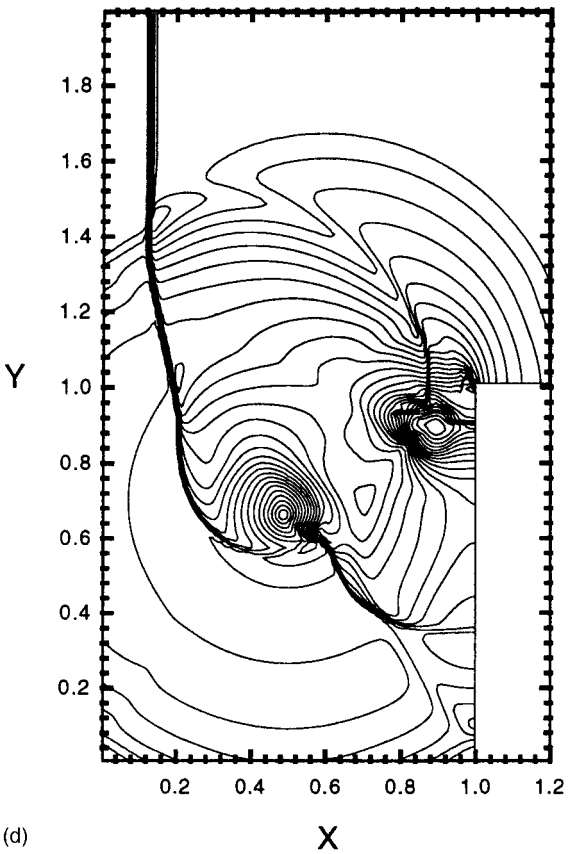

Figure 4 (*Continued*)

y-axis. The pressure jump across the shock at $x = 0.42$ to the left of the vortex center can be compared with that at $x = 0.58$ to the right, and shows the relative weakening and strengthening respectively due to the interaction with the vortex. A finite jump in pressure does not exist along $x = 0.50$ implying a local disruption in the shock structure there. In Figure 7(b), the pressure jump across the entire shock wave is compared with that of a shock wave at the same position but undisturbed by a vortex. A local one-dimensional analysis is used to obtain the pressure jump across the shock. This is a simple approximation, but on average it does provide a reasonable qualitative picture of the shock strength variation in the interaction region. The undisturbed shock has a continuously decreasing strength from its 'top' to the final position perpendicular to the wall. The disturbed shock is weaker than its undisturbed counterpart left of the vortex center ($x = 0.50$), where the vortical velocity is in the same direction as the shock velocity. To the right of the vortex center, the shock velocity is opposed by the vortex rotation causing an increase in its relative Mach number and hence of the shock strength compared with the undisturbed shock. The strength of the shock is weakest in the core region to the left of the vortex center, where the shock is almost parallel to the x-axis and the shock wave virtually vanishes. Similarly, in the core region to the right of the vortex center, where the shock is almost parallel to the x-axis, the shock strength peaks to a value comparable with that in the top planar part.

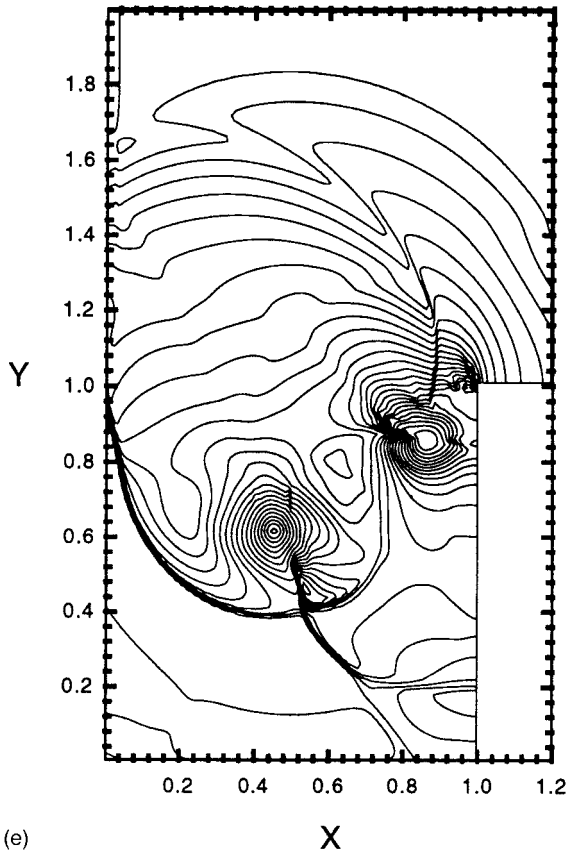

(e)

Figure 4 (*Continued*)

5. TESTS FOR NUMERICAL ACCURACY

The phenomenon of a temporary disruption of the shock wave during its interaction with a strong compressible vortex was further verified for different spatial accuracies of the numerical scheme and also on different discretizations. Numerical simulations were carried out using first-order- and second-order-accurate (in space) ENO schemes on a discretization of 300×300 grid points, in addition to using an ENO scheme of third-order spatial accuracy on the same discretization discussed previously. A third-order-accurate in space ENO scheme was also used to solve on discretizations of 600×600 and 150×150 grid points in addition to that discussed extensively for 300×300 grid points. The temporal accuracy was always of second-order.

Figure 8(a) show pressure profiles through $x = 0.5$ and parallel to the y-axis for the counter-clockwise rotating vortex in the second test case at a normalized time of 0.76 (corresponding to a local disruption in the shock structure). The pressure contours corresponding to this situation (Figure 4(c) and Figure 6) showed a disruption in the shock structure around $x = 0.5$ with the shock front almost parallel to the x-axis at that point. The pressure profiles are obtained using ENO schemes of first-, second- and third-order spatial accuracy on a discretization of 300×300 grid points. The lack of a finite pressure jump is predicted in all three cases, although the spatially first-order-accurate scheme fails to predict the drop in

pressure around the vortex center. In Figure 8(b) the same variation is presented using an ENO scheme of a third-order spatial accuracy on discretizations of 150×150, 300×300 and 600×600 grid points. The lack of a finite jump in pressure at this location is again predicted in all the three discretizations, although there is a slight underprediction of the drop in pressure around the vortex center in the coarser discretizations.

6. DISRUPTION CRITERIA

In order to establish conditions leading to a local disruption in the shock structure it is necessary to get an idea about the extent of weakening undergone by a shock wave as it encounters a flow field having a component of the flow velocity in the direction of the propagating shock wave. In the present interaction, the original diffracting shock wave experiences a maximum weakening when the peak tangential velocity of the vortex is directed along the local shock wave velocity. This effect, which may lead to a local disruption in the shock structure, is modeled as a one-dimensional idealization.

The modeling would require the characteristics of the flow field in the vortex at the time of the local disruption in the shock structure (normalized time of 0.76). Figure 9 shows the vortex

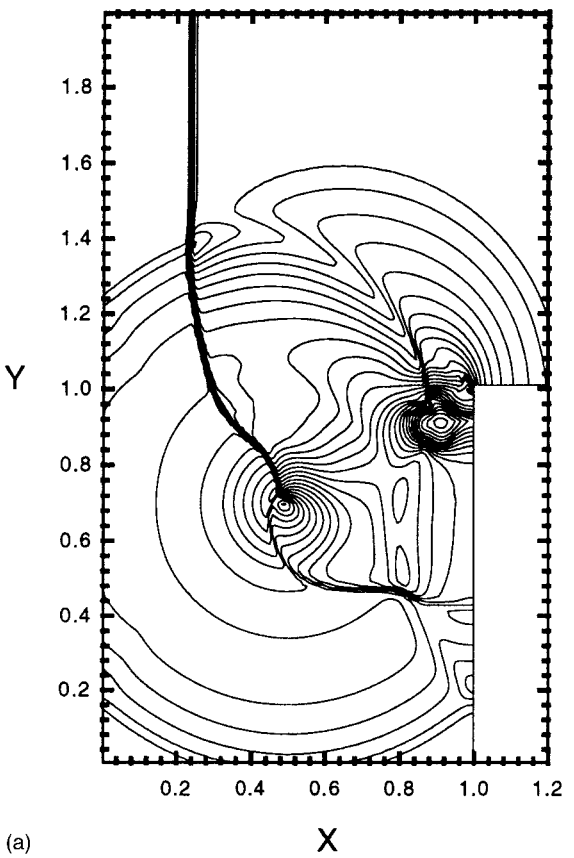

Figure 5. Pressure contours for test case 2 with clockwise rotating vortex; (a) $T = 0.76$, (b) $T = 1.04$.

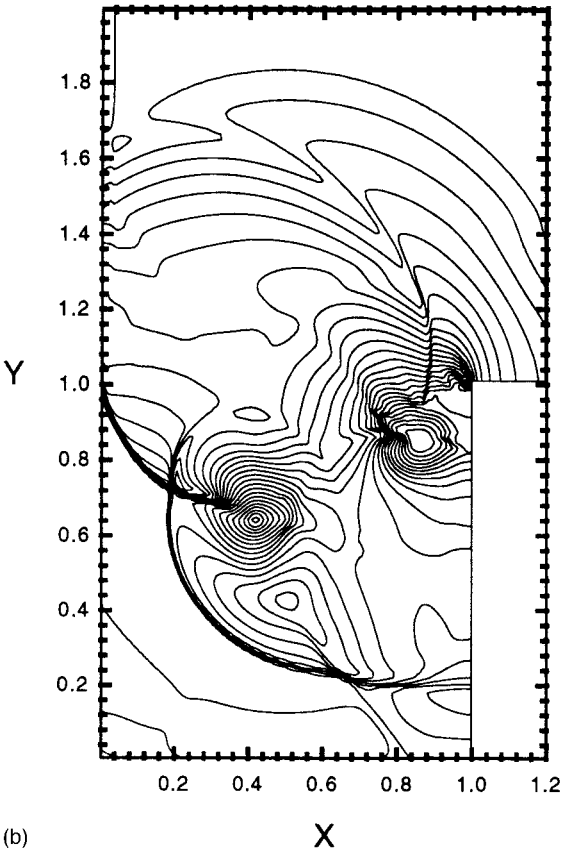

Figure 5 (*Continued*)

flow field at a normalized time of 0.76 when left to freely evolve with an initial distribution given by Equations (4) and (5), and this is used to approximate conditions prevailing in the vortex for the actual shock–vortex interaction at the time of a local disruption in the shock front. The tangential velocity distribution that develops along the radius of the vortex along with the corresponding pressure and density profiles are shown in Figure 9(a) and (b) respectively. A peak tangential velocity corresponding to a local Mach number of 0.6 can be seen in the core region of the vortex, it may be noted that this is equal to the assigned core vortex velocity U_c (Equation (4)) in the previous simulations. Both the pressure and density decrease in a similar monotonic fashion along the vortex radius. These distributions for tangential velocity, pressure and density inside the vortex are very similar to those measured experimentally for a freely moving compressible vortex [6].

In the one-dimensional idealization considered, the 'pre-interaction' shock wave had pre-shock conditions (1) (zero velocity and ambient values of pressure and density) and post-shock conditions (2) prescribed according to the Rankine–Hugoniot relations for a given incident shock wave Mach number. The pre-shock conditions (1) are then replaced by new conditions (1′) corresponding to the peak tangential velocity of Mach number 0.6 in the vortex (see Figure 9(a)) together with related values of pressure and density from Figure 9(b). To find the resultant shock wave Mach number, only a single Riemann problem between states (1′) and (2)

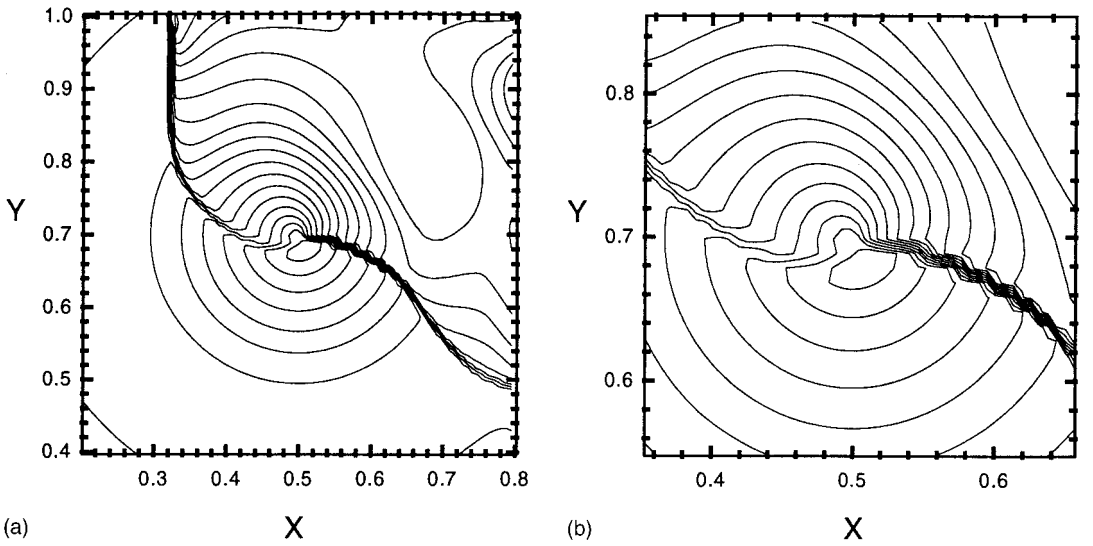

Figure 6. Pressure contours for test case 2 with counter-clockwise rotating vortex, and discretization 600×600 grid points; (a) $T = 0.76$, region of vortex; (b) $T = 0.76$, region of vortex core.

needs to be solved. Figure 10 shows the resultant relative Mach number for this shock, as a function of its initial incident Mach number. It can be seen that the shock wave will degenerate into a Mach wave for incident shock wave Mach numbers between 1.2 and 1.3. This is in good agreement with that encountered in the two-dimensional numerical simulations of the interaction between a curved shock wave and a compressible vortex having the same peak tangential velocity.

Assuming the disruption criteria to be a resultant relative Mach number of 1.015 for the propagating shock wave, the above mentioned calculations were carried out to find the incident shock wave Mach number (M_d) at which the shock wave disruption is first encountered for various peak tangential velocities of the vortex (represented by state (1′) in the calculations). In the curved shock–vortex interaction discussed previously, the core vortex velocity U_c, which also equals the peak tangential velocity for the vortex, was taken as the induced velocity behind an initially planar shock wave that propagates with Mach number M_p. This value of M_p along with the computed values of M_d are shown for various peak tangential Mach numbers of the vortex in Figure 11.

7. CONCLUSION

The interaction between a curved shock wave and a compressible vortex was numerically investigated using the ENO scheme. The curved shock was obtained by diffracting an incident planar shock around a right-angled corner and was allowed to interact with a compressible vortex superimposed on the flow. The investigation concentrated on the local deformation of the shock structure in the interaction region. This deformation depends on the placement of the vortex because of the curvature and varying strength of the shock.

The curved shock undergoes a very typical modification to its profile in the interaction region in the presence of a vortex. Because of the varying strength of the shock, the same

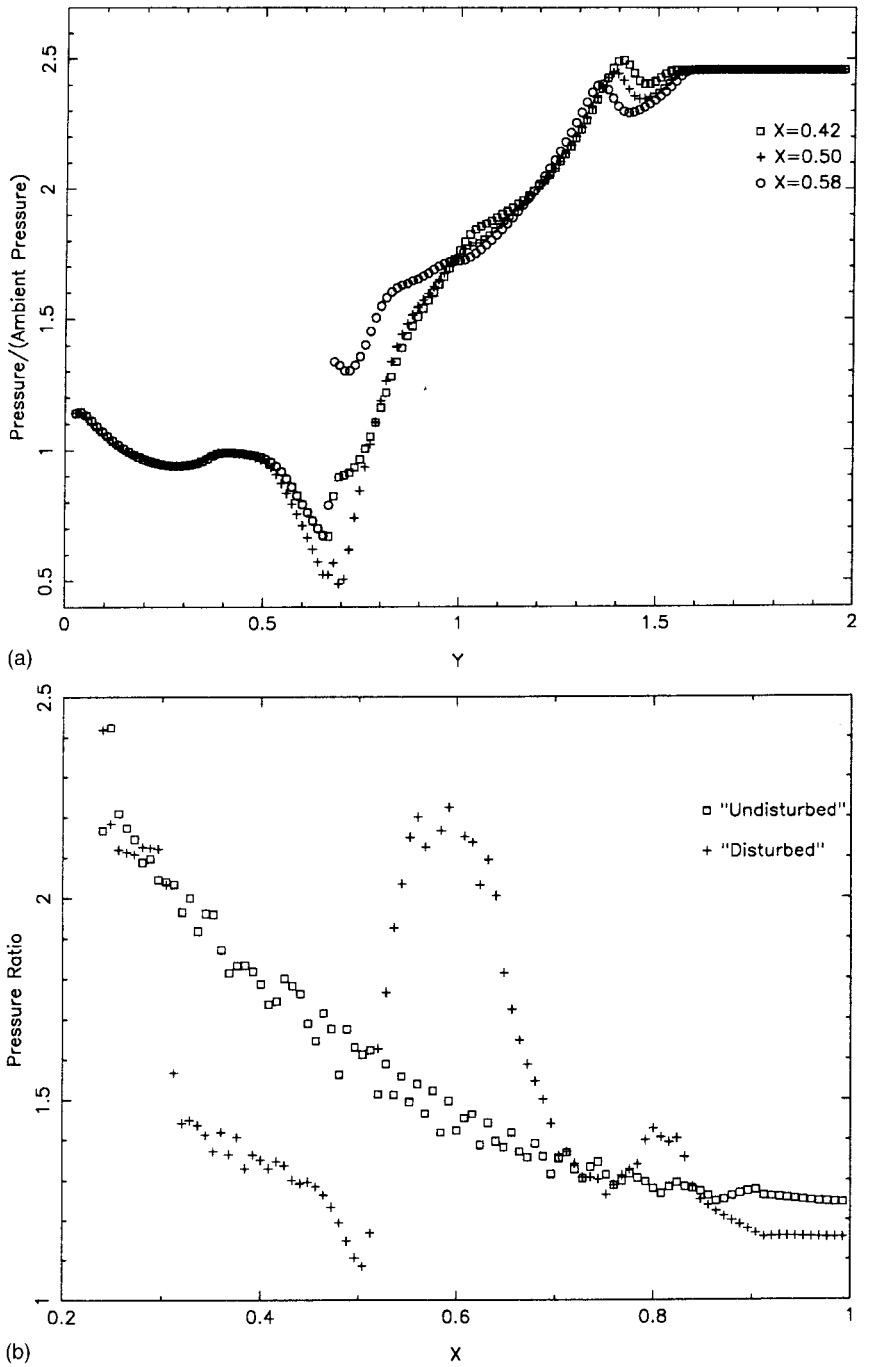

Figure 7. Pressure variations for test case 2 with counter-clockwise rotating vortex ($T = 0.76$); (a) at discrete x-stations; (b) the pressure jump compared with an undisturbed shock.

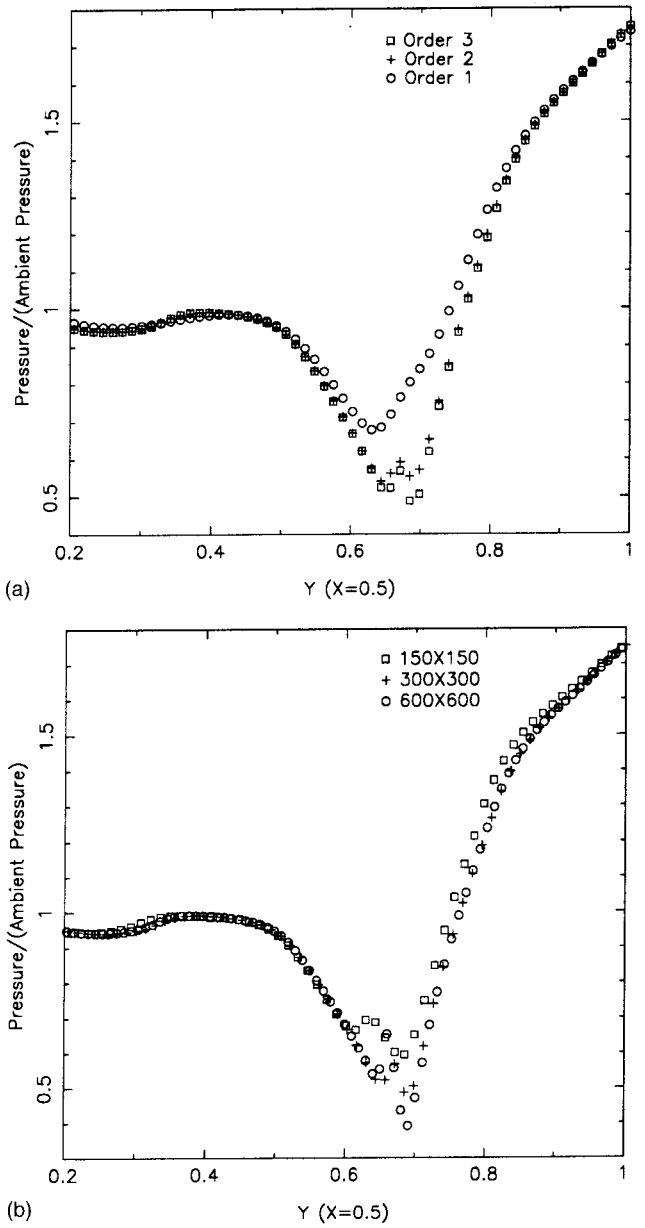

Figure 8. Tests for numerical accuracy; (a) comparison involving order of accuracy of numerical scheme; (b) comparison involving different discretizations.

vortex can cause a very different effect on the shock structure depending on the strength of the shock in the interaction region. This effect could range from a non-symmetric deformation to a temporary disruption of the shock wave in the interaction region.

The part of the shock wave that moves into a region where the fluid velocity is in the same direction as the advancing shock wave experiences a decrease in the relative Mach number and a consequent weakening of that part of the shock. If this relative Mach number approaches

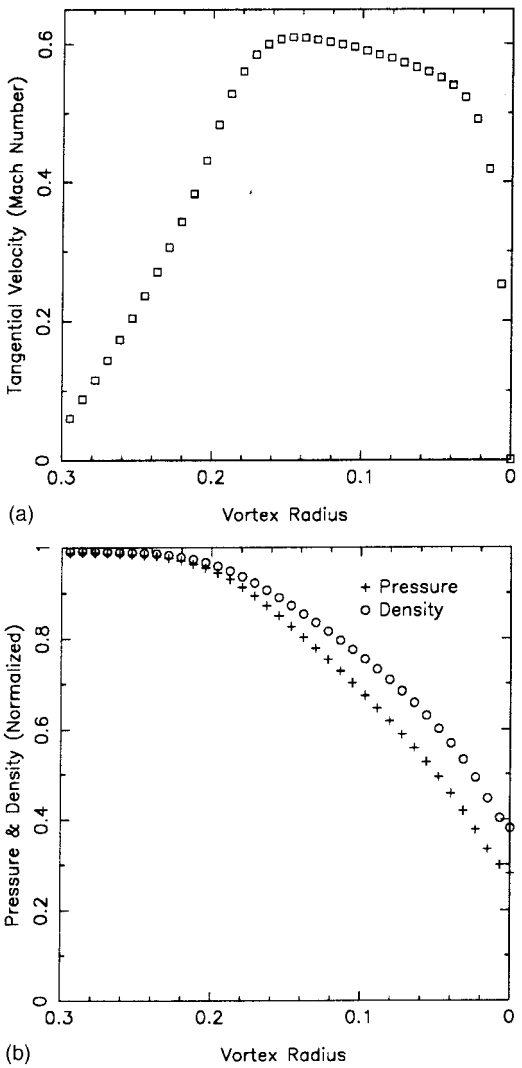

Figure 9. Particulars of free vortex; (a) tangential velocity profile; (b) pressure and density normalized with respect to ambient.

sonic values, a full scale disruption in the shock structure could occur. This weakening and a tendency towards disruption will be most prominent when a part of the shock wave has the least possible relative Mach number during the shock–vortex interaction. As noted the tendency of a counter-clockwise rotating vortex is to change the curved shock into being almost horizontal (parallel to the x-axis) in the interaction region, while the tendency of a clockwise rotating vortex is to make it almost vertical. Thus, the first disruption is most likely to occur due to a counter-clockwise rotating vortex when the shock wave is almost aligned with the vortex diameter parallel to the x-axis. In this position, the part of the shock wave left of the vortex center has the least possible relative Mach number in the interaction. For a clockwise rotating vortex, the least relative Mach number occurs when it is aligned with the vortex diameter almost parallel to the y-axis. In this position, the least relative Mach number

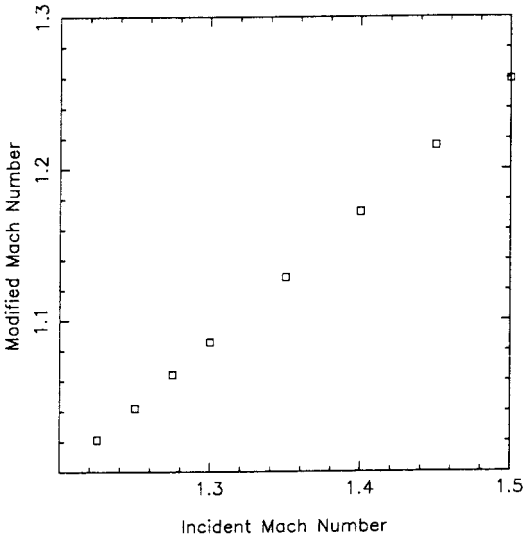

Figure 10. Shock wave Mach number for the modified and initial configuration: the resultant relative Mach number as a function of incident shock wave Mach number.

for the shock occurs below the vortex center and the initial disruption is likely to be encountered here.

This temporary disruption in the shock wave was analyzed in a more simple framework that considers planar shock waves of various incident Mach numbers (in the same range as that for the curved shock) propagating into a flow field having a velocity (corresponding to the peak tangential vortex velocity) in the same direction as the propagating shock wave. The shock wave degenerates to a Mach wave for similar values of incident Mach numbers as that

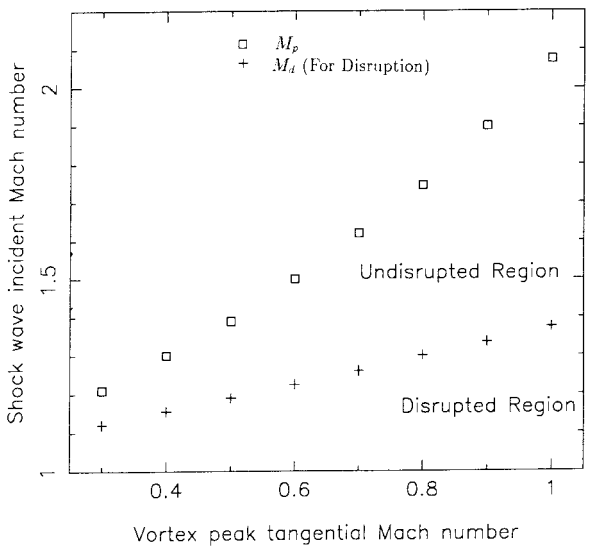

Figure 11. Incident shock wave Mach number required for disruption for various peak tangential Mach numbers of vortex.

encountered in the initial disruption process of a curved shock wave interacting with a strong compressible vortex. This shows that the tendency towards shock wave disruption in the relatively complicated case of a curved shock–vortex interaction can be predicted by simple one-dimensional considerations.

REFERENCES

1. K.R. Meadows, A. Kumar and M.Y. Hussaini, 'Computational study on the interaction between a vortex and a shock wave', *AIAA J.*, **29**, 174–179 (1991).
2. J.L. Ellzey, M.R. Henneke, J.M. Picone and E.S. Oran, 'The interaction of a shock with a vortex: shock distortion and the production of acoustic waves', *Phys. Fluids A*, **7**, 172–184 (1995).
3. L. Guichard, L. Vervisch and P. Domingo, 'Two-dimensional weak shock–vortex interaction in a mixing zone', *AIAA J.*, **33**, 1797–1802 (1995).
4. A. Harten and S. Osher, 'Uniformly high-order accurate non-oscillatory schemes I', *SIAM J. Numer. Anal.*, **24**, 279–309 (1987).
5. A. Harten, B. Engquist, S. Osher and S. Chakravarthy, 'Uniformly high-order accurate essentially non-oscillatory schemes III', *J. Comput. Phys.*, **71**, 231–303 (1987).
6. C.T. Kao, K. von Ellenrieder, R.W. MacCormack and D. Bershader, 'Physical analysis of the two-dimensional compressible vortex–shock interaction', *AIAA Paper 96–0044*, 1996.
7. O. Igra, J. Falcovitz, H. Reichenbach and W. Hellig, 'Experimental and numerical study of the interaction between a planar shock wave and a square cavity', *J. Fluid Mech.*, **313**, 105–130 (1996).
8. C. Shu and S. Osher, 'Efficient implementation of essentially non-oscillatory shock-capturing schemes', *J. Comput. Phys.*, **77**, 439–457 (1988).
9. C. Shu and S. Osher, 'Efficient implementation of essentially non-oscillatory shock-capturing schemes II', *J. Comput. Phys.*, **83**, 32–78 (1989).
10. P. Woodward and P. Collela, 'The numerical simulation of two-dimensional fluid flow with strong shocks', *J. Comput. Phys.*, **54**, 115–173 (1984).
11. C.B. Allen, 'The reduction of numerical entropy generated by unsteady shock waves', *Aeronaut. J.*, **101**, 9–16 (1997).
12. B.W. Skews, 'The shape of a diffracting shock wave', *J. Fluid Mech.*, **29**, 297–304 (1967).

